Journal of Medicinal Chemistry

Article

pubs.acs.org/jmc

Discovery of Selective LRRK2 Inhibitors Guided by Computational Analysis and Molecular Modeling

Huifen Chen,*[,†] Bryan K. Chan,[†] Jason Drummond,[‡] Anthony A. Estrada,[†] Janet Gunzner-Toste,[†] Xingrong Liu,[§] Yichin Liu,[‡] John Moffat,[‡] Daniel Shore,[†] Zachary K. Sweeney,[†,⊥] Thuy Tran,[†] Shumei Wang,[†] Guiling Zhao,[†] Haitao Zhu,[∥] and Daniel J. Burdick*[,†]

[†]Discovery Chemistry Department, [‡]Biochemical and Cellular Pharmacology Department, [§]Drug Metabolism and Pharmacokinetics Department, and [∥]Neuroscience Department, Genentech, Inc., 1 DNA Way, South San Francisco, California 94080, United States

Supporting Information

ABSTRACT: Mutations in the genetic sequence of leucine-rich repeat kinase 2 (LRRK2) have been linked to increased LRRK2 activity and risk for the development of Parkinson's disease (PD). Potent and selective small molecules capable of inhibiting the kinase activity of LRRK2 will be important tools for establishing a link between the kinase activity of LRRK2 and PD. In the absence of LRRK2 kinase domain crystal structures, a LRRK2 homology model was developed that provided robust guidance in the hit-to-lead optimization of small molecule LRRK2 inhibitors. Through a combination of molecular modeling, sequence analysis, and matched molecular pair (MMP) activity cliff analysis, a potent and selective lead inhibitor was discovered. The selectivity of this compound could be understood using the LRRK2 homology model, and application of this learning to a series of 2,4-diaminopyrimidine inhibitors in a scaffold hopping exercise led to the identification of highly potent and selective LRRK2 inhibitors that were also brain penetrable.

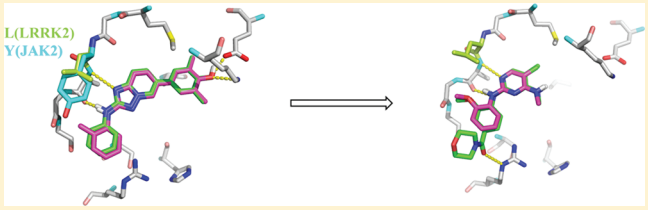

INTRODUCTION

Parkinson's disease (PD) is a multisystem neurodegenerative disorder that is clinically characterized primarily by tremors, rigidity, and bradykinesia.[1] The current standard of care for PD patients is limited to symptomatic treatment, which only provides temporary attenuation of motor symptoms and does not affect the progression of neurodegeneration. There is, therefore, a strong demand for disease modifying or neuroprotective therapies. One of the more attractive targets for disease modification was identified in 2004 when genetic variations in the LRRK2 gene were linked to familial PD.[2,3] In particular, the specific G2019S mutation of LRRK2 has been associated with both familial and idiopathic PD.[4−6] The LRRK2 gene encodes a large protein with multiple domains, including a kinase domain.[7−9] The detailed physiological function and effectors of the LRRK2 kinase are largely unknown and remain to be determined.[10] Importantly, the G2019S mutation in the kinase domain is a dominant mutation that has been shown to increase LRRK2 kinase activity in vitro, suggesting that the kinase activity of LRRK2 is involved in Parkinson's disease pathophysiogenesis.[11−14] Indeed, recent studies with nonspecific LRRK2 small molecule inhibitors have suggested that inhibition of LRRK2 activity might ameliorate neurodegenerative phenotypes in *C. elegans* and *Drosophila* Parkinson's disease models and mouse models of LRRK2.[15,16] However, because of the lack of general kinase selectivity of compounds used in the efficacy studies, the biological effects of LRRK2 kinase inhibition remain to be elucidated.[17]

A few selective inhibitors of LRRK2 kinase activity such as LRRK2-IN-1[18] and CZC-25146[19] have been described recently. However, they do not appear to have sufficient CNS exposure to be used in mammalian models of PD. A potent ALK/LRRK2 kinase inhibitor, TAE684, was recently reported to achieve significant brain exposure in mouse but did not inhibit LRRK2 phosphorylation in the brain.[20] The development of selective and brain penetrable LRRK2 inhibitors therefore remains a critical need for the LRRK2 field.[21] In this contribution, we describe our initial efforts to use structure-based design and computational approaches to identify useful LRRK2 chemical probes starting from a high-throughput screening effort.

RESULTS

A high-throughput screening campaign using G2019S LRRK2 protein[22] yielded a number of interesting small molecule inhibitor scaffolds, including triazolopyridines and diaminopyrimidines represented by compounds **1** and **2** (Figure 1). The triazolopyridine compounds were highly potent and had physical properties consistent with CNS penetration,[23] while the aminopyrimidine inhibitors had excellent ligand efficiency (LE).[24,25] It is well-known, however, that the diaminopyrimidine motif is particularly well-represented in the kinase inhibition literature[26] and the potential selectivity of these compounds was a concern. We therefore focused our initial computer-aided design efforts on the development of models

Received: March 31, 2012
Published: May 16, 2012

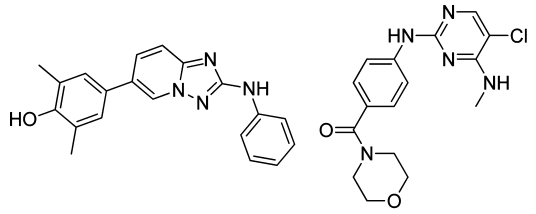

1

MW = 330
TPSA = 62
cLogP = 5.5
LRRK2 K_i = 20 nM
LE = 0.42
LipE = 2.2

2

MW = 348
TPSA = 79
cLogP = 2.1
LRRK2 K_i = 6 nM
LE = 0.47
LipE = 6.1

Figure 1. Chemical structures of high-throughput screening hits **1** and **2**.

and approaches that would allow us to improve the selectivity of compounds such as **1** and **2**.

Homology Modeling and ATP-Binding Site Analysis. Use of crystal structure information is critical to the success of a structure-based drug design (SBDD) effort. However, the structure of the kinase domain of LRRK2 has not yet been reported.[27] Therefore, construction of a LRRK2 homology model[7,10,28−30] using known kinase structures as templates was initiated. The most crucial elements for building a homology model are the choice of structural templates and sequence alignment.[31−33] The choice of template can be influenced by numerous factors including sequence identity and functional relevance to the target protein, structural quality, and purpose of the model. Since our goal was to use the homology model for SBDD, we had to be even more prudent with the selection of structural templates in order to generate a model that would allow the docking of most LRRK2 inhibitors.

Two approaches were employed to identify appropriate structural templates. The first approach relied on using kinase domain (KD) crystal structures of proteins that have a high degree of sequence homology with the KD of LRRK2.[34] Using Psi-Blast,[35] a panel of human protein kinases with the highest KD sequence identity to LRRK2 was identified (Table 1), although none of the kinases have sequence identity to LRRK2 greater than 32%. Several homology models were built with MLK1, TIE2, and TAK1 protein structures as templates using MOE (Chemical Computing Group, Inc.).[36] The models built with these templates were useful for elucidating general features of the ATP binding site, such as hinge residues, gatekeeper, and other residues that could participate in ATP and/or inhibitor binding. However, none of them proved robust enough to provide reasonable docking poses for all of the top priority chemical classes found in the screening campaign.

The second approach for template selection was to search for kinases that exhibited similar inhibition profiles as LRRK2 for a given set of inhibitors. Analysis of the internal biochemical activity profiles of LRRK2 inhibitors found in the screening campaign revealed a surprising correlation between LRRK2 and JAK3 and a weaker correlation with JAK2. These data suggested that JAK3 crystal structures could be good structural templates for building LRRK2 homology models. However, because of the paucity of available high quality JAK3 crystal structures, JAK2 cocrystal structures were used. The final LRRK2 model (Figure 2A) was constructed from an unpublished in-house JAK2 cocrystal structure similar to a published structure (PDB code 3JY9).[37] The JAK2 structure was chosen based on its very high resolution (1.7 Å) and open ATP-binding site, which would allow the docking of many diverse compounds without introducing steric clashes. Similar to other protein kinases, the LRRK2 KD consists of a smaller N-terminal lobe and a larger C-terminal lobe connected by the hinge. According to the model, the N-terminal domain consists mostly of β sheets and an α helix, while the C-terminal domain consists of mostly α helices. The ATP-binding site is situated at the interface of the two lobes. The gatekeeper, Met1947, and catalytic residues, Lys1906 and Glu1920, line the back wall of the ATP-binding site, while residues Glu1948, Leu1949, and Ala1950 form the side wall along the kinase hinge (Figure 2B). The side chains of amino acids Phe1883, Leu1885, Val1893, and Ala1904 form the ceiling of the ATP site, and those of Ile1933, Gly1953, Ser1954, and Leu2001 form the floor. At the opening of ATP-binding site, the side chains of Arg1957 and His1998 partially close in on the sugar moiety of ATP. The binding pocket is relatively closed and flat along the hinge and becomes more open near the solvent exposed region as well as the sugar and phosphate binding region. The ATP-binding pocket is largely hydrophobic with the exception of the hinge

Table 1. Multiple Sequence Alignment of ATP-Binding Site Residues[a] of LRRK2 and Selected Kinases

Kinase/ LRRK2 Residue Number	kinase domain (ATP site) Seq ID	Phe 1883	Leu 1885	Phe 1890	Val 1893	Ala 1904	Lys 1906	Phe 1908	Glu 1920	Leu 1924	Ile 1933	[b]Met 1947	Leu 1949	Ala 1950	Gly 1953	Ser 1954	Arg 1957	Asn 1999	Leu 2001	Ala 2016	Asp 2017
LRRK2		F	L	F	V	A	K	F	E	L	I	M	L	A	G	S	R	N	L	A	D
LRRK1	32 (60)	S	L	S	I	A	K	F	E	L	V	L	L	A	S	S	T	N	L	S	D
MLK1	32 (65)	E	I	F	V	A	K	H	E	F	I	M	F	A	G	P	R	N	L	T	D
TIE2	31 (65)	D	I	F	V	A	K	M	E	L	I	I	Y	A	G	N	D	N	L	A	D
BRAF	30 (45)	Q	I	F	V	A	K	L	E	L	L	T	W	C	S	S	H	N	F	G	D
TAK1	29 (65)	E	V	F	V	A	K	S	E	L	V	M	Y	A	G	S	N	N	L	C	D
SRC	29 (60)	V	L	F	V	A	K	L	E	M	V	T	Y	M	G	S	D	N	L	A	D
JAK3	27 (65)	S	L	F	V	A	K	L	E	L	V	M	Y	L	G	C	D	N	L	A	D
JAK2	26 (65)	Q	L	F	V	A	K	L	E	L	V	M	Y	L	G	S	D	N	L	G	D
IRAK1	26 (55)	L	I	F	V	A	K	L	E	L	V	Y	F	L	G	S	D	N	L	G	D
ROCK1	23 (55)	K	I	F	V	A	K	L	E	M	V	M	Y	M	G	D	N	N	L	A	D

[a]Residue numbers are based on Swiss-Prot nomenclature.[34] Cells colored in red have identical amino acids as in LRRK2. [b]Gatekeeper residue.

dx.doi.org/10.1021/jm300452p | J. Med. Chem. 2012, 55, 5536−5545

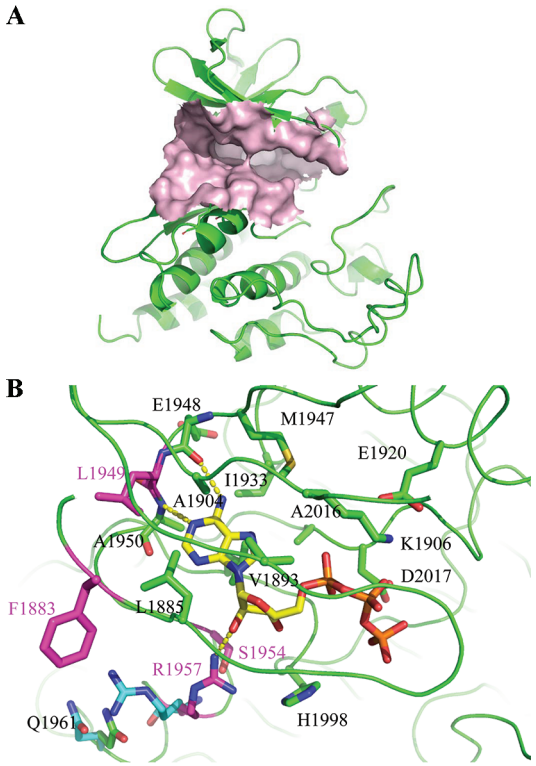

Figure 2. (A) LRRK2 kinase domain homology model with the N-terminal domain on top and C-terminal domain at bottom. The solvent accessible surface of the ATP-binding site is colored in pink, while the cartoon defining the protein backbone is colored in green. (B) LRRK2 ATP-binding site in complex with ATP (colored in yellow) looking down through the N-terminal domain. Side chains of binding site residues are shown as sticks and colored in green. Side chains of the four key selectivity residues (Phe1883, Leu1949, Ser1954, and Arg1957) are colored in magenta. The alternative conformations of Arg1957 and Gln1961 are shown in cyan. Hydrogen bond interactions between ATP and LRRK2 are shown as yellow dashed lines.

backbone hydrogen bond donor/acceptors, back pocket Lys1906 and Glu1920, and the front pocket Arg1957 side chain.

To investigate the validity of the LRRK2 model for structure-based design purposes, extensive docking studies on a diverse set of LRRK2 inhibitors, including those reported in the literature[29,38] and those found in the high-throughput screen, were initiated. Reasonable docking models could be generated for most of the LRRK2 inhibitors either by using the automatic docking program Glide (Schrödinger, Inc.)[39] or by manually docking inhibitors in the LRRK2 homology model. The side chain conformations of Arg1957 and Gln1961 prevented the docking of some inhibitors, so a second LRRK2 model was generated by moving these mobile side chains out of the inhibitor binding site (Figure 2B). These two models were used in lieu of a crystal structure to guide our design efforts.

Identification of molecular basis that determines kinase selectivity[40−45] is an important aspect of kinase drug discovery research because of the highly conserved kinase domain structures and ATP binding sites across the human kinome.[46] LRRK2 KD has low sequence identity to other protein kinases and even its closest related family member, LRRK1,[28,47] has a KD sequence identity of only 32% (Table 1). The ATP-binding site of LRRK2, however, is more conserved and has much higher sequence identity to other protein kinases. In an effort to identify protein residues that could impart kinase selectivity, a detailed binding site sequence analysis was performed (Table 1). Out of the 19 binding site residues whose side chains could potentially interact with ATP-competitive inhibitors, six are conserved in over 400 kinases, five are conserved in 200−300 kinases, and eight are conserved in less than 150 kinases. To identify residues with the highest likelihood to confer selectivity against other kinases, we analyzed the relative locations, accessibility, and properties of the eight least conserved residues and narrowed the list down to four residues: Phe1883, Leu1949, Ser1954, and Arg1957.

Phe1883 is removed from the ATP-binding site and at the interface of the solvent exposed region. This residue is something other than phenylalanine in over 350 kinases and could perhaps be contacted by inhibitors with larger groups. Leu1949 presents the most attractive selectivity handle because of its proximity to the hinge binding moiety and its shorter side chain relative to the dominant Phe or Tyr side chains in approximately 290 other kinases.[48,49] The smaller Leu side chain creates a small cavity in LRRK2 that is not present in most other kinases and could be exploited to improve kinase selectivity. Similarly, there are over 230 kinases with a side chain larger than Ser1954, and of those, 200 have either a Glu or Asp side chain. Arg1957 provides another residue to target for selectivity with approximately 200 kinases containing a negatively charged Asp or Glu side chain. We hypothesized that

Table 2. Matched-Pair Activity Cliffs Identified from the Triazolopyridine JAK2 Activity Cliff Analysis

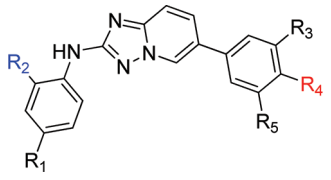

pair	compd	R_1	R_2	R_3	R_4	R_5	JAK2 K*i* (μM)	JAK2 activity ratio
A	3	-COOH	-H	$-CH_3$	-OH	$-CH_3$	0.0004	1862
	4				-H		0.745	
B	5	-COOH	-H	-H	-OH	-H	0.024	133
	6				$-CH_3$		3.2	
C	5	-COOH	-H	-H	-OH	-H	0.024	112
	7				$-SO_2CH_3$		2.7	
D	1	-H	-H	$-CH_3$	-OH	$-CH_3$	0.003	135
	8		$-CH_3$				0.405	

dx.doi.org/10.1021/jm300452p | J. Med. Chem. 2012, 55, 5536−5545

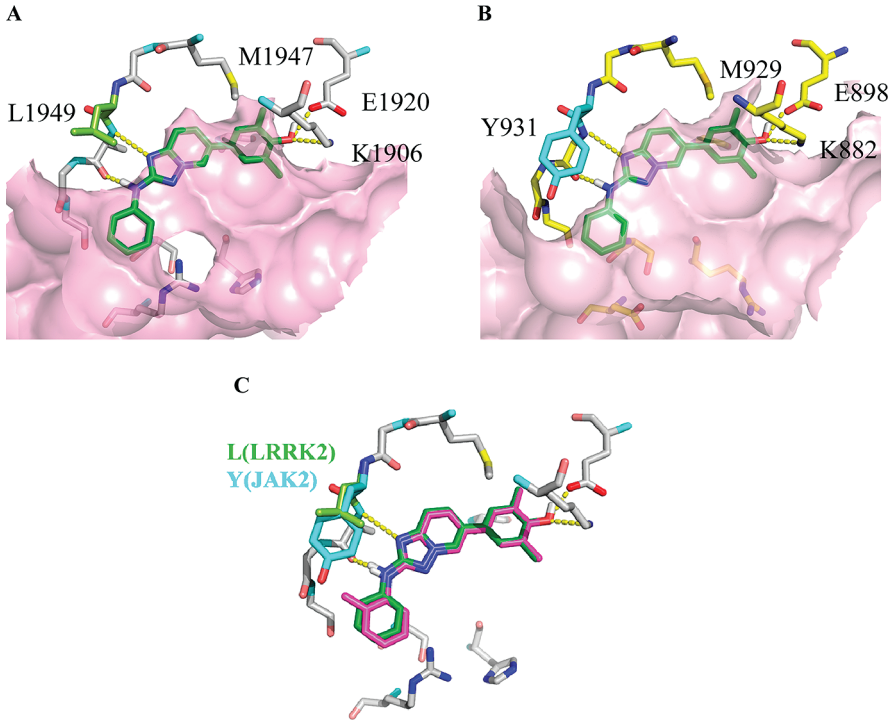

Figure 3. (A) Docking model of compound **1** (green) in LRRK2 binding site. Key hydrogen bonds are shown in yellow dashed lines. Solvent accessible surface is shown in pink. (B) Docking model of compound **1** in JAK2. (C) Overlay of compound **1** (green) and **8** (magenta) docking models in LRRK2 (colored in white with L1949 in green). The side chain of Y931 of JAK2 is also shown and colored in cyan.

targeting one or more of these four residues was a good strategy[50] to achieve general kinase selectivity and potency of the small molecule inhibitors.

Identification of Selectivity Hotspot through Matched-Pair Analysis. The triazolopyridine hit **1** was an attractive starting point for further optimization owing to its good LRRK2 potency (K_i = 20 nM) and high ligand efficiency (LE = 0.42); however, it was found to inhibit JAK2 with a K_i of 3 nM. To evaluate whether JAK2 selectivity could be achieved in this series, a substructure search of our internal compound library using the unsubstituted version of **1** (Table 2, R_1−R_5 = H) was performed. One-hundred compounds containing the substructure were tested in a JAK2 inhibition assay, and the data were analyzed using MMP[51−56] to uncover structural features associated with significantly reduced JAK2 potency.

For the matched-pair analysis, a Tanimoto similarity coefficient of 0.94 was used as a cutoff to identify closely related pairs. The cutoff JAK2 K_i for being considered inactive was 250 nM. Out of the 100 tested compounds, 320 compound pairs were identified that met the chemical space similarity criteria. For a pair to be considered to have an activity cliff, the biological activity ratio had to be at least 2 orders of magnitude. Only four pairs met the activity ratio criteria as shown in Table 2. Three of the four pairs (A, B, and C) involved a replacement of the hydroxyl (R_4) with a hydrogen, methyl, or methyl sulfone, all of which led to a significant loss of JAK2 activity. The last pair (D, compounds **1** and **8**) was not substituted in the same manner as the other three pairs. An additional methyl group on the aniline (R_2) portion of compound **8** greatly reduced the activity of the inhibitor against JAK2 in comparison to compound **1**.

Compound **1** was docked to the ATP-binding site of the LRRK2 homology model. Models of this compound in the ATP-binding site of LRRK2 and JAK2 are shown in Figure 3A and Figure 3B. Several key interactions could account for the excellent LRRK2 and JAK2 potency of **1**. The 2-aminotriazole core binds to the adenine site and forms a pair of strong hydrogen bonds to the hinge backbone in addition to numerous hydrophobic interactions with residues above and below the core. The 3,5-dimethyl-4-phenol moiety binds in the mostly hydrophilic back pocket, with the hydroxyl accepting one hydrogen bond from the conserved catalytic Lys1906 while donating one to the conserved Glu1920 in helix C of LRRK2 (residues Lys882 and Glu898 of JAK2). The phenol ring also makes hydrophobic interactions with gatekeeper Met1947 in LRRK2 and Met929 in JAK2. The unsubstituted aniline ring binds to a hydrophobic channel that leads to the solvent exposed region of the ATP site in both proteins. On the basis of this binding mode, replacement of the 4-hydroxyl of the phenol would be difficult, since it acts as both a donor and acceptor to two highly conserved catalytic residues. All three matched-pair compounds **4**, **6**, and **7** involved replacement of this hydroxyl which resulted in significant loss in JAK2 potency. As this subpocket of LRRK2 is nearly identical to that of JAK2, a similar loss in LRRK2 potency would be expected to occur.

The loss in activity in the last matched pair (D), does not involve a hydroxyl replacement but rather an addition of a methyl to the aniline portion of the molecule. As shown in Figure 3B, the unsubstituted aniline of compound **1** fits tightly against the JAK2 protein surface formed by the hinge and side chain of Tyr931. An ortho-methyl substitution on the phenyl ring could clash with Tyr931 and cause a significant drop in JAK2 potency. This observation is consistent with the 135-fold drop in JAK2 activity seen in compound **8**. An inspection of the LRRK2 protein surface (Figure 3A) indicates that the methyl of compound **8** might fit well in the pocket created by the smaller side chain of Leu1949 in LRRK2, a key selectivity residue that was suggested by the ATP binding site analysis. Indeed,

dx.doi.org/10.1021/jm300452p | J. Med. Chem. 2012, 55, 5536−5545

compound **8** was 2-fold more potent ($K_i \approx 10$ nM) than compound **1** in the LRRK2 binding assay, indicating that the pocket formed by Leu1949 can provide a selectivity handle.

In an effort to confirm that JAK2 selectivity is a good indicator of overall kinase selectivity in this series, compound **8** was tested against an Invitrogen panel of 63 kinases (Supporting Information Table 1). Consistent with the hypothesis, compound **8** was very selective and only inhibited one kinase (Abl) in addition to wild-type and mutant G2019S LRRK2 at greater than 50% inhibition at 1 μM. These data strongly support the proposed binding mode and the hypothesis that general kinase selectivity can be achieved in this series by introducing small groups in the vicinity of the Leu1949 side chain. However, optimization of the triazolopyridine scaffold was not pursued because of difficulties in maintaining potency and good physicochemical properties while replacing the 3,5-dimethyl-4-hydroxyphenyl moiety.

Optimization of the Diaminopyrimidines. The diaminopyrimidine series identified in the HTS campaign (**2**, Figure 1) had excellent biochemical potency and ligand efficiency. The physicochemical properties also represented reasonable starting points for a series designed to cross the blood–brain barrier. However, for this scaffold to advance as a lead series, significant improvement of the selectivity profile was needed.

The suggested binding mode of compound **2** in the LRRK2 homology model is shown in Figure 4A. The 2,4-diaminopyrimidine core binds to the adenine site and interacts with the kinase hinge through a pair of hydrogen bonds to the backbone amide NH and carbonyl oxygen of Ala1950. According to our model, the C5 chlorine forms favorable van der Waals interactions with the Met1947 gatekeeper side chain, and the C4 N-methyl fills a hydrophobic cavity. The carbonyl oxygen of the amide group forms a weak hydrogen bond with the guanidinium side chain of Arg1957, with nonideal hydrogen bond geometry. The aniline ring binds in a flat hydrophobic cleft along the hinge near the opening of the ATP-binding site with the 4-morpholinoamide group pointing toward the side chain of Phe1883.

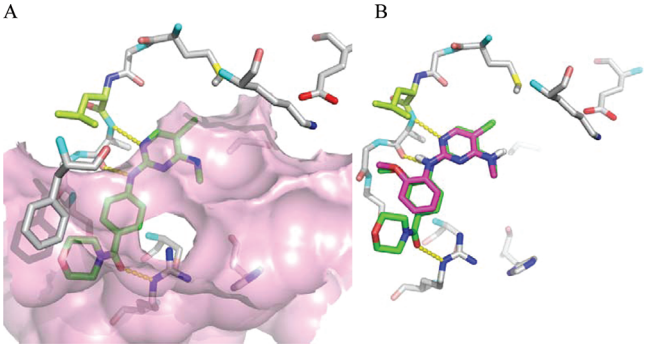

Figure 4. (A) Docking model of compound **2** (green) in LRRK2 binding site. (B) Overlay of docking models of compound **11** (magenta) and **15** (green) in LRRK2 binding site. Intermolecular hydrogen bonds are shown as dashed yellow lines, while the solvent accessible surface is shown in pink. Leu1949 is shown in light green sticks.

On the basis of the docking model, we hypothesized the following: (1) the front pocket morpholino amide could possibly be removed without a significant impact on LRRK2 potency; (2) compound **2** might be a nonselective kinase inhibitor, since it binds to the same hinge region as compound **1** and does not access the Leu1949 selectivity pocket; (3) the selectivity of this class of compounds could be significantly improved by ortho-substitution on the aniline ring. Compound **2** was tested in the JAK2 assay and found to be a potent inhibitor of JAK2 kinase activity (Table 4). The truncated compound **9** was also tested in both the LRRK2 and JAK2 binding assays (Table 3). Loss of the morpholino amide resulted in a 2-fold loss in potency against LRRK2 and a 9-fold loss in potency against JAK2. These data suggested that the molecular weight and TPSA of this series could be significantly reduced and that this series could lead to the discovery of compounds with properties consistent with CNS penetration.

Table 3. LRRK2 Activity and JAK2 Selectivity of Ortho-Substituted Front Pocket Phenyl Diaminopyrimidines

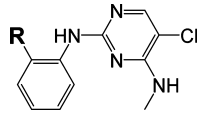

		K_i (μM)		
compd	R	LRRK2	JAK2	JAK2/LRRK2 index
9	H	0.011	0.064	6
10	CH_3	0.020	>3.2	>160
11	OCH_3	0.006	>3.2	>533
12	Br	0.033	>3.2	>97
13	$OCHF_2$	0.007	>3.2	>457

Using knowledge of structure–selectivity relationships gained from the triazolopyridines, a methyl group was installed in the ortho position of the aniline moiety in the truncated series (compound **10**, Table 3). Although there was a slight loss in potency against LRRK2, significant selectivity against JAK2 was achieved. It appeared from the homology model that the pocket near Leu1949 was small and that large groups, such as a phenyl, would not fit. Small substituents were tolerated to varying degrees (Table 3). The methyl (**10**) and Br (**12**) substitutions caused a 2- to 3-fold drop in LRRK2 potency, while the methoxy (**11**) and difluoromethoxy (**13**) groups led to slight improvement in LRRK2 potency. More importantly, all of the ortho-substituted compounds, **10**–**13**, achieved greater than 97-fold selectivity over JAK2 in comparison to the unsubstituted compound **9**. These same trends were observed when the same ortho-substitutions were incorporated into the original HTS hit (**14**–**16**, Table 4). First, the morpholinoamide analogues had the same potency rank order seen with the truncated analogues. The slight loss in activity seen with compound **9** was regained with the addition of the morpholinoamide. Second, the compounds were very selective against JAK2, with the methoxy substituent achieving over 1000-fold selectivity against JAK2. This result supports the idea that the methoxy group fits favorably in the pocket near Leu1949.

To further confirm that filling the Leu1949 pocket maintained selectivity against JAK2, several substitutions were made at the C5 position of the pyrimidine core (Table 4). As predicted by the binding mode of compound **2**, R_1 can modulate the LRRK2 biochemical potency (**17**–**20**) through van der Waals interactions, conformational preference, and electronic effects, without having any obvious impact on JAK2 activity. Replacement with the smaller and more electronegative fluorine (**18**) reduced LRRK2 activity by 24-fold and substitution with a nitrile (**20**) by 4-fold. Interestingly,

dx.doi.org/10.1021/jm300452p | J. Med. Chem. 2012, 55, 5536–5545

Table 4. LRRK2 Activity and JAK2 Selectivity of Ortho-Substituted Front Pocket Phenyl Morpholinoamide Diaminopyrimidines

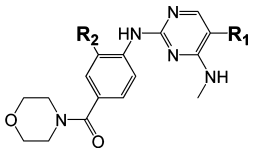

			K_i (μM)		
compd	R_1	R_2	LRRK2	JAK2	JAK2/LRRK2 index
2	Cl	H	0.006	0.007	1
14	Cl	CH_3	0.007	>3.2	>457
15	Cl	OCH_3	0.003	>3.2	>1067
16	Cl	Br	0.013	>3.2	>246
17	Br	OCH_3	0.001	3.0	>3000
18	F	OCH_3	0.071	>3.2	>45
19	CF_3	OCH_3	0.001	>3.2	>3200
20	CN	OCH_3	0.013	>3.2	>246

replacement with a bromine (**17**) or CF_3 (**19**) increased potency by 3-fold. Compound **15** was tested against a panel of 63 kinases at Invitrogen (Supporting Information Table 1). As shown previously with compound **8**, compound **15** inhibits only wild-type and G2019S mutant LRRK2 at greater than 50% inhibition at 1 μM and it does not inhibit Abl. This result further validated the hypothesis that installation of substituents in the small selectivity pocket near Leu1949 could impart general kinase selectivity.

As there is a critical need for a potent, selective, and brain penetrable LRRK2 tool compound, the ability of compound **15** to cross the blood–brain barrier in rodents was assessed based on its favorable physicochemical properties (cLogP, TPSA, and CNS MPO score of 1.9, 88 Å^2, and 5.4, respectively). **15** was evaluated in wild-type (FVB) and P-gp/BCRP knockout mice[57,58] following a 1 mg/kg intravenous injection. The total brain to plasma AUC ratios and the unbound brain to unbound plasma AUC ratios were 1.4 and 0.61, respectively, in wild-type and 2.9 and 1.3, respectively, in P-gp/Bcrp knockout mice. The half-life ($T_{1/2}$) was 0.23 h. At 1 h following 30 mg/kg intraperitoneal injection in wild-type mouse, the total and unbound plasma concentrations of compound **15** were 8.4 and 1.1 μM, respectively, and the total and unbound brain concentrations were 6.2 and 0.37 μM, respectively. While these data suggest that P-gp and/or Bcrp slightly restrict the brain penetration in mice for **15**, it clearly demonstrates that this compound achieves desirable brain penetration for use as a tool compound in animal models of PD.

Chemistry. The target compounds were synthesized as depicted in Scheme 1. Commercially available 2,4-dichloropyrimidines were reacted with 8 M methylamine in ethanol at room temperature to produce intermediates **26**–**30**. 2,5-Dichloro-*N*-methylpyrimidin-4-amine **27** and appropriately substituted anilines were suspended in *n*-butanol and subjected to microwave irradiation to yield products **9**–**13**.

The appropriately substituted 4-aminobenzoic acids were coupled to morpholine using standard amide bond chemistry to generate intermediates **31**–**34**. These intermediates were then coupled to the proper 2-chloropyrimidine, **26**–**30**, via acid catalyzed S_NAr to yield products **2** and **14**–**20**.

CONCLUSION

In the absence of LRRK2 KD crystal structures, we relied on homology modeling as a viable way to provide a 3D LRRK2 model that can be used for structure-based design. The choice of structural templates proved to be critical to yield a model robust for structure-based design. We found that structures with the highest sequence identity to LRRK2 (e.g., MLK1, Tie2, Braf) were not the best choice for homology modeling owing to factors such as paucity of high resolution cocomplex structures, partially hindered binding sites or conformational states not represented in target protein. What proved particularly useful was the analysis of available selectivity data,

Scheme 1[a]

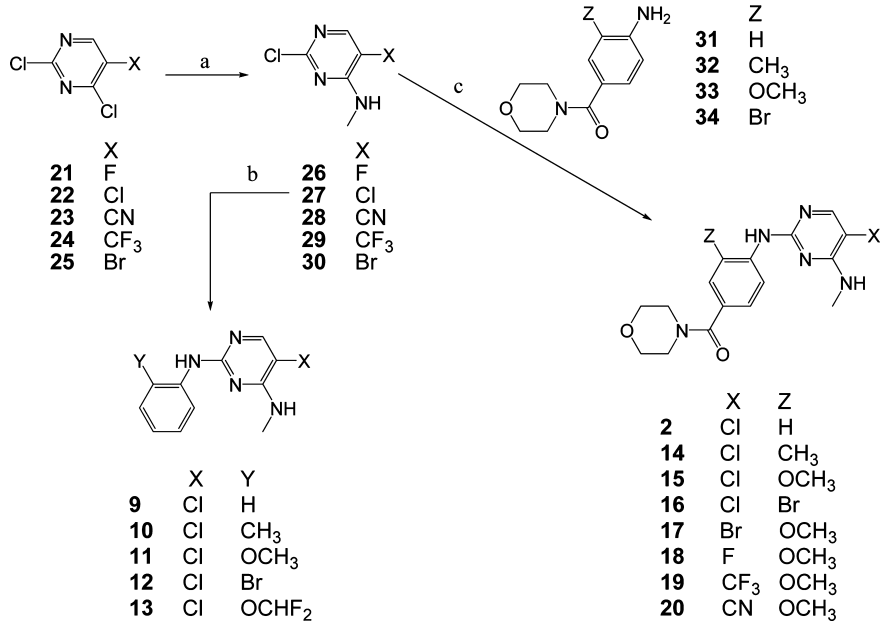

[a](a) 8 M methylamine in ethanol, methanol; (b) Ar-NH_2, *n*-butanol; (c) TFA, 2-methoxyethanol.

dx.doi.org/10.1021/jm300452p | J. Med. Chem. 2012, 55, 5536–5545

which revealed an unexpected correlation between inhibition of JAK3/2 and LRRK2. This result led to the choice of JAK2 as a structural template for modeling despite relatively low sequence identity (26%) between LRRK2 and JAK2. The particular choice of JAK2 structure can also have an impact on the robustness of the homology model. We chose a high resolution JAK2 structure with an open ATP-binding site, which proved very useful for docking a diverse set of LRRK2 small molecule inhibitors. The LRRK2 homology models have been used in conjunction with binding site sequence analysis and MMP activity cliff analysis to identify residues that can potentially impart general kinase selectivity. One such residue is Leu1949, which is mostly a Phe or Tyr in other protein kinases. By incorporation of small substituents on an otherwise nonselective kinase inhibitor to reach the small selectivity pocket created by Leu1949 in LRRK2, broad kinase selectivity can be achieved. Through molecular modeling guided medicinal chemistry efforts, the nonselective 2,4-diaminopyridine hit **2** was optimized into a promising lead series and compounds in this series are being used to probe the link between LRRK2 kinase activity and Parkinson's disease. Details of this work are forthcoming.

EXPERIMENTAL SECTION

General Methods. All solvents and reagents were used as obtained from the commercial vendors. Intermediates were purified on a Teledyne ISCO CombiFlash system using prepacked silica gel columns using appropriate gradients of ethyl acetate and heptane unless otherwise noted. All final products were purified by preparative reverse phase HPLC using appropriate gradients of acetonitrile and water with 0.05% formic acid as the counterion. All tested compounds were determined to be >95% pure by high-performance liquid chromatography under the following conditions: system, Agilent 1200 series HPLC instrument equipped with an Agilent 6140 quadrapole mass spectrometer; column, Agilent C18 (2.1 mm × 30 mm, 1.8 μm); flow rate 0.4 mL/min; mobile phase A, deionized water; mobile phase B, 0.05% trifluoroacetic acid in acetonitrile; gradient, 3% B (0−0.5 min), 3−95% B (0.5−7.0 min), 95% B (7.0−7.5 min), 3% B (7.5−7.6 min). Purity was calculated as a percentage of total areas at 254 nm. ^{1}H NMR spectra were recorded using a Bruker Avance III 400 MHz or Bruker Avance III 500 MHz spectrometer. Chemical shifts are in parts per million (δ) referenced to Me_4Si (0.00 ppm). Liquid chromatography electrospray mass spectra were recorded using a Sciex 150EX LC−MS system with a Shimadzu LC10AD liquid chromatograph.

2-Chloro-5-fluoro-*N*-methylpyrimidin-4-amine (26). Methylamine (8 M in ethanol, 15 mL, 120 mmol) was added to 5-fluoro-2,4-dichloropyrimidine (**21**, 9.0 g, 53.9 mmol) in methanol (40 mL). The mixture was stirred at room temperature and then concentrated under reduced pressure. The residue was purified by silica gel chromatography using a methanol/dichloromethane gradient of 1−10% over 35 min to give pure 2-chloro-5-fluoro-*N*-methylpyrimidin-4-amine (**26**, 6.77 g, 77.7%) as an off white solid. ^{1}H NMR (400 MHz, DMSO) δ 8.14 (s, 1H), 8.04 (d, J = 3.5 Hz, 1H), 2.85 (d, J = 4.6 Hz, 3H); ESMS m/z 162.6 (M + 1).

In a similar fashion, the following intermediates were synthesized from the appropriate starting materials using the procedure for **26**.

2,5-Dichloro-*N*-methylpyrimidin-4-amine (27). ^{1}H NMR (500 MHz, DMSO) δ 8.13 (s, 1H), 2.87 (d, J = 4.6 Hz, 4H); ESMS m/z 178.9 (M + 1).

2-Chloro-4-(methylamino)pyrimidine-5-carbonitrile (28). ^{1}H NMR (500 MHz, $CDCl_3$) δ 8.31 (s, 1H), 5.74 (s, 1H), 3.34 (d, J = 5 Hz, 3H); ESMS m/z 171.7 (M + 1).

2-Chloro-*N*-methyl-5-(trifluoromethyl)pyrimidin-4-amine (29). ^{1}H NMR (400 MHz, DMSO) δ 8.37 (s, 1H), 7.91 (s, 1H), 2.90 (d, J = 4.5 Hz, 3H); ESMS m/z 212.1 (M + 1).

5-Bromo-2-chloro-*N*-methylpyrimidin-4-amine (30). ^{1}H NMR (400 MHz, DMSO) δ 8.21 (s, 1H), 7.71 (s, 1H), 2.86 (d, J = 4.6 Hz, 4H); ESMS m/z 224.0 (M + 1).

5-Chloro-N^4-methyl-N^2-phenylpyrimidine-2,4-diamine (9). 2,5-Dichloro-*N*-methylpyrimidin-4-amine (**27**, 0.06 g, 0.337 mmol), aniline (0.063 g, 0.674 mmol), and *n*-butanol (0.8 mL) were placed in a 10 mL CEM microwave vial. The vial was capped and irradiated in a CEM microwave reactor for 20 min at 150 °C followed by concentration under reduced pressure. The residue was purified by preparative reverse phase HPLC to give 5-chloro-N^4-methyl-N^2-phenylpyrimidine-2,4-diamine (**9**, 0.0076 g, 9.6%) as an off white solid: ^{1}H NMR (500 MHz, DMSO) δ 9.14 (s, 1H), 7.91 (s, 1H), 7.75 (d, J = 7.7 Hz, 2H), 7.30−7.19 (m, 2H), 7.13 (d, J = 3.9 Hz, 1H), 6.89 (t, J = 7.3 Hz, 1H), 2.92 (d, J = 4.6 Hz, 3H); ESMS m/z 235.0 (M + 1).

In a similar fashion, the following compounds were synthesized from the appropriate starting materials using the procedure for **9**.

5-Chloro-N^4-methyl-N^2-*o*-tolylpyrimidine-2,4-diamine (10). ^{1}H NMR (400 MHz, DMSO) δ 8.20 (s, 1H), 7.80 (s, 1H), 7.56 (d, J = 7.9 Hz, 1H), 7.19−7.07 (m, 2H), 7.07−6.92 (m, 2H), 2.81 (d, J = 4.6 Hz, 3H), 2.21 (s, 3H); ESMS m/z 249.1 (M + 1).

5-Chloro-N^2-(2-methoxyphenyl)-N^4-methylpyrimidine-2,4-diamine (11). ^{1}H NMR (400 MHz, DMSO) δ 8.30 (dd, J = 7.4, 2.0 Hz, 1H), 7.92 (s, 1H), 7.56 (s, 1H), 7.22 (d, J = 4.2 Hz, 1H), 7.04−6.97 (m, 1H), 6.93 (dd, J = 9.4, 3.8 Hz, 2H), 3.86 (s, 3H), 2.90 (d, J = 4.6 Hz, 3H); ESMS m/z 265.0 (M + 1).

N^2-(2-Bromophenyl)-5-chloro-N^4-methylpyrimidine-2,4-diamine (12). ^{1}H NMR (400 MHz, DMSO) δ 8.08−7.97 (m, 2H), 7.89 (s, 1H), 7.62 (d, J = 8.0 Hz, 1H), 7.35 (t, J = 7.7 Hz, 1H), 7.22 (d, J = 4.3 Hz, 1H), 7.00 (t, J = 7.6 Hz, 1H), 2.85 (d, J = 4.6 Hz, 3H); ESMS m/z 314.9 (M + 1).

5-Chloro-N^2-(2-(difluoromethoxy)phenyl)-N^4-methylpyrimidine-2,4-diamine (13). ^{1}H NMR (400 MHz, DMSO) δ 8.17−8.12 (m, 1H), 7.95 (s, 1H), 7.90 (s, 1H), 7.27−7.17 (m, 3H), 7.14 (t, J = 74 Hz, 1H), 7.09−7.02 (m, 1H), 2.87 (d, J = 4.6 Hz, 3H); ESMS m/z 301.0 (M + 1).

(4-Amino-3-methoxyphenyl)(morpholino)methanone (33). 4-Amino-3-methoxybenzoic acid (0.50 g, 2.99 mmol), *N*-(3-dimethylaminopropyl)-*N*′-ethylcarbodiimide hydrochloride (1.43 g, 7.48 mmol), 1-hydroxybenzotriazole (0.606 g, 4.49 mmol), *N*,*N*-diisopropylethylamine (1.56 mL, 8.97 mmol), morpholine (2.608 mL, 29.9 mmol), and *N*,*N*-dimethylformamide (15 mL) were combined and stirred for 18 h at room temperature. The mixture was concentrated under reduced pressure and the residue partitioned between ethyl acetate (50 mL) and water (50 mL). The aqueous layer was extracted with ethyl acetate (30 mL), and the combined organic extracts were washed with saturated sodium chloride (30 mL), dried over $MgSO_4$, and concentrated under reduced pressure. The residue was purified by silica gel chromatography using an ethyl acetate/heptane gradient of 0−100% over 15 min to give (4-amino-3-methoxyphenyl)(morpholino)methanone (**33**, 0.505 g, 71.4%) as a glassy solid. ^{1}H NMR (400 MHz, DMSO) δ 6.85 (s, 1H), 6.80 (d, J = 8.0 Hz, 1H), 6.61 (d, J = 8.0 Hz, 1H), 5.12 (s, 2H), 3.77 (s, 3H), 3.57 (d, J = 4.2 Hz, 4H), 3.50 (d, J = 4.4 Hz, 4H); ESMS m/z 237.2 (M + 1).

In a similar fashion, the following intermediates were synthesized from the appropriate starting materials using the procedure for **33**.

(4-Aminophenyl)(morpholino)methanone (31). ^{1}H NMR (400 MHz, DMSO) δ 7.13 (d, J = 8.3 Hz, 2H), 6.54 (d, J = 8.3 Hz, 2H), 5.49 (s, 2H), 3.57 (d, J = 4.5 Hz, 4H), 3.48 (d, J = 4.7 Hz, 4H); ESMS m/z 207.2 (M + 1).

(4-Amino-3-methylphenyl)(morpholino)methanone (32). ^{1}H NMR (400 MHz, DMSO) δ 7.03 (s, 1H), 7.00 (d, J = 8.2 Hz, 1H), 6.58 (d, J = 8.1 Hz, 1H), 5.26 (s, 2H), 3.56 (d, J = 4.1 Hz, 4H), 3.48 (d, J = 4.2 Hz, 4H), 2.05 (s, 3H); ESMS m/z 221.3 (M + 1).

(4-Amino-3-bromophenyl)(morpholino)methanone (34). ^{1}H NMR (400 MHz, DMSO) δ 7.44 (s, 1H), 7.17 (d, J = 8.3 Hz, 1H), 6.80 (d, J = 8.3 Hz, 1H), 5.76 (s, 2H), 3.58 (d, J = 4.2 Hz, 4H), 3.50 (d, J = 4.0 Hz, 4H); ESMS m/z 285.1 (M + 1).

(4-(5-Chloro-4-(methylamino)pyrimidin-2-ylamino)phenyl)-(morpholino)methanone (2). 2,5-Dichloro-*N*-methylpyrimidin-4-

amine (**27** 0.10 g, 0.562 mmol), (4-aminophenyl)(morpholino)-methanone (**33**, 0.348 g, 1.69 mmol), trifluoroacetic acid (0.1 mL, 1.35 mmol), and 2-methoxyethanol (2 mL) were combined and heated for 18 h 125 °C. The mixture was concentrated under reduced pressure and the residue was purified by preparative reverse phase HPLC to give (4-(5-chloro-4-(methylamino)pyrimidin-2-ylamino)phenyl)-(morpholino)methanone (**2**, 0.051 g, 25.8%) as an off white solid: ^{1}H NMR (400 MHz, DMSO) δ 9.46 (s, 1H), 7.95 (s, 1H), 7.83 (d, J = 8.6 Hz, 2H), 7.32 (d, J = 8.6 Hz, 2H), 7.25 (d, J = 4.6 Hz, 1H), 3.67–3.40 (m, 8H), 2.94 (t, J = 7.0 Hz, 3H); ESMS m/z 348.1 (M + 1).

In a similar fashion, the following compounds were synthesized from the appropriate starting materials using the procedure for **2**.

(4-(5-Chloro-4-(methylamino)pyrimidin-2-ylamino)-3-methylphenyl)(morpholino)methanone (14). ^{1}H NMR (400 MHz, DMSO) δ 8.32 (s, 1H), 7.86 (s, 1H), 7.76 (d, J = 8.2 Hz, 1H), 7.23 (s, 1H), 7.19 (d, J = 8.3 Hz, 1H), 7.13 (d, J = 4.5 Hz, 1H), 3.54 (d, J = 38.0 Hz, 8H), 2.84 (d, J = 4.6 Hz, 3H), 2.26 (s, 3H); ESMS m/z 362.1 (M + 1).

(4-(5-Chloro-4-(methylamino)pyrimidin-2-ylamino)-3-methoxyphenyl)(morpholino)methanone (15). ^{1}H NMR (400 MHz, DMSO) δ 8.41 (d, J = 8.2 Hz, 1H), 7.96 (s, 1H), 7.68 (s, 1H), 7.32 (d, J = 4.1 Hz, 1H), 7.05 (s, 1H), 7.01 (d, J = 8.2 Hz, 1H), 3.90 (s, 3H), 3.56 (d, J = 34.5 Hz, 8H), 2.90 (t, J = 7.3 Hz, 3H); ESMS m/z 378.1 (M + 1).

(3-Bromo-4-(5-chloro-4-(methylamino)pyrimidin-2-ylamino)phenyl)(morpholino)methanone (16). ^{1}H NMR (400 MHz, DMSO) δ 8.21 (d, J = 8.5 Hz, 1H), 8.06 (s, 1H), 7.94 (s, 1H), 7.67 (d, J = 1.6 Hz, 1H), 7.41 (d, J = 8.5 Hz, 1H), 7.32 (d, J = 4.4 Hz, 1H), 3.55 (d, J = 41.3 Hz, 8H), 2.88 (d, J = 4.6 Hz, 3H); ESMS m/z 428.0 (M + 1).

(4-(5-Bromo-4-(methylamino)pyrimidin-2-ylamino)-3-methoxyphenyl)(morpholino)methanone (17). ^{1}H NMR (400 MHz, DMSO) δ 8.40 (d, J = 8.3 Hz, 1H), 8.04 (s, 1H), 7.68 (s, 1H), 7.14 (d, J = 4.6 Hz, 1H), 7.05 (d, J = 1.6 Hz, 1H), 7.01 (dd, J = 8.3, 1.6 Hz, 1H), 3.90 (s, 3H), 3.56 (d, J = 34.6 Hz, 8H), 2.90 (d, J = 4.6 Hz, 3H); ESMS m/z 422.0 (M + 1).

(4-(5-Fluoro-4-(methylamino)pyrimidin-2-ylamino)-3-methoxyphenyl)(morpholino)methanone (18). ^{1}H NMR (400 MHz, DMSO) δ 8.46 (d, J = 8.3 Hz, 1H), 7.89 (d, J = 3.6 Hz, 1H), 7.56 (d, J = 5.5 Hz, 2H), 7.04 (s, 1H), 7.00 (d, J = 8.3 Hz, 1H), 3.90 (s, 3H), 3.58 (d, J = 19.4 Hz, 4H), 3.52 (s, 3H), 2.90 (t, J = 7.7 Hz, 3H); ESMS m/z 362.1 (M + 1).

(3-Methoxy-4-(4-(methylamino)-5-(trifluoromethyl)-pyrimidin-2-ylamino)phenyl)(morpholino)methanone (19). ^{1}H NMR (400 MHz, DMSO) δ 8.31 (d, J = 8.2 Hz, 1H), 8.19 (s, 1H), 8.07 (s, 1H), 7.21 (d, J = 4.3 Hz, 1H), 7.07 (s, 1H), 7.02 (d, J = 8.2 Hz, 1H), 3.90 (s, 3H), 3.56 (d, J = 37.1 Hz, 9H), 2.92 (d, J = 4.3 Hz, 3H); ESMS m/z 412.1 (M + 1).

2-(2-Bromo-4-(morpholine-4-carbonyl)phenylamino)-4-(methylamino)pyrimidine-5-carbonitrile (20). ^{1}H NMR (400 MHz, DMSO) δ 8.33 (d, J = 5.9 Hz, 2H), 8.18 (d, J = 8.2 Hz, 1H), 7.76 (d, J = 4.3 Hz, 1H), 7.08 (d, J = 1.5 Hz, 1H), 7.04–6.97 (m, 1H), 3.88 (s, 3H), 3.56 (d, J = 37.1 Hz, 8H), 2.88 (d, J = 4.5 Hz, 3H); ESMS m/z 369.1 (M + 1).

Microfluidic Capillary Electrophoresis Assay. LRRK2 reactions were carried out in a final volume of 10 μL per well in a 384-well microplate. A standard enzymatic mixture, for which the reaction was initiated by the addition of 5 μL of 2× ATP to 5 μL of 2× enzyme, contained 10 nM G2019S, 1 μM FAM-LRRKtide (5FAM-GAGRLGRDKYKTLRQIRQ-CONH$_2$), 130 μM ATP, 25 mM Tris, pH 8.0, 5 mM $MgCl_2$, 0.01% Triton X-100, 2 mM DTT, 5 mM β-glycerophosphate, 5 mM NaF,100 μM Na_3VO_4, and 1× protease inhibitor cocktail (Calbiochem). After incubation for 120 min at ambient temperature, the product and substrate in each reaction were separated using a 12-sipper microfluidic chip (Caliper Life Sciences, Hopkinton, MA) run on a Caliper LC3000 (Caliper Life Sciences, Hopkinton, MA). The separation of product and substrate was optimized by choosing voltages and pressure using Caliper's optimizer software (Hopkinton, MA). The separation buffer contained 100 mM HEPES, pH 7.2, 0.015% Brij-35, 0.1% coating reagent 3, 10 mM EDTA, and 5% DMSO. The separation conditions used a downstream voltage of −500 V, an upstream voltage of −2350 V, and a screening pressure of −1.4 psi. The product and substrate fluorescence was excited at 488 nm and detected at 530 nm. Substrate conversion was calculated from the electrophoregram using HTS Well Analyzer software (Caliper Life Sciences, Hopkinton, MA).

Brain Penetration Protocol. For the brain penetration studies, plasma and brain tissues were collected at 5 min and 1 h following the intravenous injection of compound **15** at 1 mg/kg in wild-type (FVB) and P-gp/Bcrp knockout mice (n = 3). The concentrations in the plasma and brain samples were determined by LC–MS/MS after sample treatment. The area under the curve (AUC) from time zero to 1 h was calculated using the trapezoidal rule. The mouse plasma and brain tissue binding were determined using equilibrium dialysis.

Molecular Modeling. Homology models of LRRK2 were constructed using the modeling program MOE, version 2009.10 (Chemical Computing Group, Montreal),[36] and AMBER99[59] force field. The human LRRK2 sequence was retrieved from Swiss-Prot[34] and aligned to template structure sequences using ClustalW[60] followed by manual fine-tuning of residues adjacent to loop regions, insertions, and deletions. The models were further refined with bound ligand using the Macromodel utility implemented in Maestro and OPLS2005 force field (Schrödinger, Inc., New York, NY).[39] Inhibitor docking studies were carried out using docking program Glide SP with one hydrogen bond constraint to the carbonyl oxygen of hinge residue Ala1950. The docking poses were evaluated based on a combination of criteria including the Glide docking score (cutoff = −6), favorable intermolecular interactions with the hinge and other parts of the ATP-binding pocket, low strain energy of the bound ligand (E_{strain} < 2 kcal/mol), etc.

Activity Cliff Analysis. Activity cliff analysis was carried out using a Pipeline Pilot protocol (Accelrys Inc.)[61] that computes pairwise Tanimoto similarities and activity changes between all pairs of compounds. The Tanimoto similarities were calculated using extended connectivity fingerprints configured with counts (ECFC_2).[62] Only pairs that met a similarity cutoff of 0.94 were analyzed for activity cliffs.

■ ASSOCIATED CONTENT

Supporting Information

Table 1 listing Invitrogen kinase selectivity profiling data. This material is available free of charge via the Internet at http://pubs.acs.org.

■ AUTHOR INFORMATION

Corresponding Author

*For H.C. and D.J.B.: phone, 650-225-1000; fax, 650-467-5155; e-mail, chen.huifen@gene.com (H.C.) and burdick.dan@gene.com (D.J.B).

Present Address

⊥Novartis Institutes for Biomedical Research (NIBR), 4560 Horton Street, Emeryville, CA 94608-2916.

Notes

The authors declare no competing financial interest.

■ ACKNOWLEDGMENTS

We thank Drs. Nicholas Skelton and Steven Magnuson for critical reading of the manuscript and helpful discussions. We also thank the analytical, bioanalytical, NMR, pharmacokinetic, and biopharmacology colleagues for their assistance with compound purification and testing.

■ ABBREVIATIONS USED

LRRK2, leucine-rich repeat kinase 2; PD, Parkinson's disease; JAK2, Janus kinase 2; JAK3, Janus kinase 3; MMP, matched

molecular pair; LE, ligand efficiency; KD, kinase domain; SBDD, structure-based drug design

REFERENCES

(1) Lees, A. J.; Hardy, J.; Revesz, T. Parkinson's disease. *Lancet* **2009**, *373*, 2055−2066. Erratum in *Lancet* **2009**, *374*, 684.

(2) Zimprich, A.; Biskup, S.; Leitner, P.; Lichtner, P.; Farrer, M.; Lincoln, S.; Kachergus, J.; Hulihan, M.; Uitti, R. J.; Calne, D. B.; Stoessl, A. J.; Pfeiffer, R. F.; Patenge, N.; Carbajal, I. C.; Vieregge, P.; Asmus, F.; Muller-Myhsok, B.; Dickson, D. W.; Meitinger, T.; Strom, T. M.; Wszolek, Z. K.; Gasser, T. Mutations in LRRK2 cause autosomal-dominant parkinsonism with pleomorphic pathology. *Neuron* **2004**, *44*, 601−607.

(3) Paisan-Ruiz, C.; Jain, S.; Evans, E. W.; Gilks, W. P.; Simon, J.; van der Brug, M.; Lopez de Munain, A.; Aparicio, S.; Gil, A. M.; Khan, N.; Johnson, J.; Martinez, J. R.; Nicholl, D.; Carrera, I. M.; Pena, A. S.; de Silva, R.; Lees, A.; Marti-Masso, J. F.; Perez-Tur, J.; Wood, N. W.; Singleton, A. B. Cloning of the gene containing mutations that cause PARK8-linked Parkinson's disease. *Neuron* **2004**, *44*, 595−600.

(4) Dachsel, J. C.; Farrer, M. J. LRRK2 and Parkinson disease. *Arch. Neurol.* **2010**, *67*, 542−547.

(5) Satake, W.; Nakabayashi, Y.; Mizuta, I.; Hirota, Y.; Ito, C.; Kubo, M.; Kawaguchi, T.; Tsunoda, T.; Watanabe, M.; Takeda, A.; Tomiyama, H.; Nakashima, K.; Hasegawa, K.; Obata, F.; Yoshikawa, T.; Kawakami, H.; Sakoda, S.; Yamamoto, M.; Hattori, N.; Murata, M.; Nakamura, Y.; Toda, T. Genome-wide association study identifies common variants at four loci as genetic risk factors for Parkinson's disease. *Nat. Genet.* **2009**, *41*, 1303−1307.

(6) Simón-Sánchez, J.; Schulte, C.; Bras, J. M.; Sharma, M.; Gibbs, J. R.; Berg, D.; Paisan-Ruiz, C.; Lichtner, P.; Scholz, S. W.; Hernandez, D. G.; Krüger, R.; Federoff, M.; Klein, C.; Goate, A.; Perlmutter, J.; Bonin, M.; Nalls, M. A.; Illig, T.; Gieger, C.; Houlden, H.; Steffens, M.; Okun, M. S.; Racette, B. A.; Cookson, M. R.; Foote, K. D.; Fernandez, H. H.; Traynor, B. J.; Schreiber, S.; Arepalli, S.; Zonozi, R.; Gwinn, K.; van der Brug, M.; Lopez, G.; Chanock, S. J.; Schatzkin, A.; Park, Y.; Hollenbeck, A.; Gao, J.; Huang, X.; Wood, N. W.; Lorenz, D.; Deuschl, G.; Chen, H.; Riess, O.; Hardy, J. A.; Singleton, A. B.; Gasser, T. Genome-wide association study reveals genetic risk underlying Parkinson's disease. *Nat. Genet.* **2009**, *41*, 1308−1312.

(7) Mata, I. F.; Wedemeyer, W. J.; Farrer, M. J.; Taylor, J. P.; Gallo, K. A. LRRK2 in Parkinson's disease: protein domains and functional insights. *Trends Neurosci.* **2006**, *29*, 286−293.

(8) Greggio, E.; Cookson, M. R. Leucine-rich repeat kinase 2 mutations and Parkinson's disease: three questions. *ASN Neuro* **2009**, *1* (e00002), 13−24.

(9) Gandhi, P. N.; Chen, S. G.; Wilson-Delfosse, A. L. Leucine-rich repeat kinase 2 (LRRK2): a key player in the pathogenesis of Parkinson's disease. *J. Neurosci. Res.* **2009**, *87*, 1283−1295.

(10) Drolet, R. E.; Sanders, J. M.; Kern, J. T. Leucine-rich repeat kinase 2 (LRRK2) cellular biology: a review of recent advances in identifying physiological substrates and cellular functions. *J. Neurogenet.* **2011**, *25*, 140−151.

(11) West, A. B.; Moore, D. J.; Biskup, S.; Bugayenko, A.; Smith, W. W.; Ross, C. A.; Dawson, V. L.; Dawson, T. M. Parkinson's disease-associated mutations in leucine-rich repeat kinase 2 augment kinase activity. *Proc. Natl. Acad. Sci. U.S.A.* **2005**, *102*, 16842−16847.

(12) Greggio, E.; Jain, S.; Kingsbury, A.; Bandopadhyay, R.; Lewis, P.; Kaganovich, A.; van der Brug, M. P.; Beilina, A.; Blackinton, J.; Thomas, K. J.; Ahmad, R.; Miller, D. W.; Kesavapany, S.; Singleton, A.; Lees, A.; Harvey, R. J.; Harvey, K.; Cookson, M. R. Kinase activity is required for the toxic effects of mutant LRRK2/dardarin. *Neurobiol. Dis.* **2006**, *23*, 329−341.

(13) Cookson, M. R. The role of leucine-rich repeat kinase 2 (LRRK2) in Parkinson's disease. *Nat. Rev. Neurosci.* **2010**, *11*, 791−797.

(14) Rudenko, I. N.; Chia, R.; Cookson, M. R. Is inhibition of kinase activity the only therapeutic strategy for LRRK2-associated Parkinson's disease? *BMC Med.* **2012**, *10*, 20−27.

(15) Liu, Z.; Hamamichi, S.; Lee, B. D.; Yang, D.; Ray, A.; Caldwell, G. A.; Caldwell, K. A.; Dawson, T. M.; Smith, W. W.; Dawson, V. L. Inhibitors of LRRK2 kinase attenuate neurodegeneration and Parkinson-like phenotypes in *Caenorhabditis elegans* and *Drosophila* Parkinson's disease models. *Hum. Mol. Genet.* **2011**, *20*, 3933−3942.

(16) Lee, B. D.; Shin, J.-H.; VanKampen, J.; Petrucelli, L.; West, A. B.; Ko, H. S.; Lee, Y.-I.; Maguire-Zeiss, K. A.; Bowers, W. J.; Federoff, H. J.; Dawson, V. L.; Dawson, T. M. Inhibitors of leucine-rich repeat kinase-2 protect against models of Parkinson's disease. *Nat. Med.* **2010**, *16*, 998−1000.

(17) Garcia-Serna, R.; Mestres, J. Chemical Probes for biological systems. *Drug Discovery Today* **2011**, *16*, 99−106.

(18) Deng, X.; Dzamko, N.; Prescott, A.; Davies, P.; Liu, Q.; Yang, Q.; Lee, J.-D.; Patricelli, M. P.; Nomanbhoy, T. K.; Alessi, D. R.; Gray, N. S. Characterization of a selective inhibitor of the Parkinson's disease kinase LRRK2. *Nat. Chem. Biol.* **2011**, *7*, 203−205.

(19) Ramsden, N.; Perrin, J.; Ren., Z.; Lee, B. D.; Zinn, N.; Dawson, V. L.; Tam, D.; Bova, M.; Lang, M.; Drewes, G.; Bantscheff, M.; Bard, F.; Dawson, T. M.; Hopf, C. Chemoproteomics-based design of potent LRRK2-selective lead compounds that attenuate Parkinson's disease-related toxicity in human neurons. *ACS Chem. Biol.* **2011**, *6*, 1021−1028.

(20) Zhang, J.; Deng, X.; Choi, H. G.; Alessi, D. R.; Gray, N. S. Characterization of TAE684 as a potent LRRK2 kinase inhibitor. *Bioorg. Med. Chem. Lett.* **2012**, *22*, 1864−1869.

(21) Kramer, T.; Lo Monte, F.; Goering, S.; Okala Amombo, G. M.; Schmidt, B. Small molecule kinase inhibitors for LRRK2 and their application to parkinson's disease models. *ACS Chem. Neurosci.* **2012**, *3*, 151−160.

(22) Lovitt, B; Vanderporten, E. C.; Sheng, Z.; Zhu, H.; Drummond, J.; Liu, Y. Differential effects of divalent manganese and magnesium on the kinase activity of leucine-rich repeat kinase 2 (LRRK2). *Biochemistry* **2010**, *49*, 3092−3100.

(23) Wager, T. T.; Hou, X.; Verhoest, P. R.; Villalobos, A. Moving beyond rules: the development of a central nervous system multiparameter optimization (CNS MPO) approach to enable alignment of druglike properties. *ACS Chem. Neurosci.* **2010**, *1*, 435−449.

(24) Hopkins, A. L.; Groom, C. R.; Alex, A. Ligand efficiency: a useful metric for lead selection. *Drug Discovery Today* **2004**, *9*, 430−431.

(25) Leeson, P. D.; Springthorpe, B. The influence of drug-like concepts on decision-making in medicinal chemistry. *Nat. Rev. Drug Discovery* **2007**, *6*, 881−890.

(26) Moore, W. J.; Richard, D.; Thorarensen, A. An analysis of the diaminopyrimidine patent estates describing spleen tyrosine kinase inhibitors by Rigel and Portola. *Expert Opin. Ther. Pat.* **2010**, *20*, 1703−1722.

(27) Deng, J.; Lewis, P. A.; Greggio, E.; Sluch, E.; Beilina, A.; Cookson, M. R. Structure of the ROC domain from the Parkinson's disease-associated leucine-rich repeat kinase 2 reveals a dimeric GTPase. *Proc. Natl. Acad. Sci. U.S.A.* **2008**, *105*, 1499−1504.

(28) Marín, I. The Parkinson disease gene LRRK2: evolutionary and structural insights. *Mol. Biol. Evol.* **2006**, *23*, 2423−2433.

(29) Nichols, R. J.; Dzamko, N.; Hutti, J. E.; Cantley, L. C.; Deak, M.; Moran, J.; Bamborough, P.; Reith, A. D.; Alessi, D. R. Substrate specificity and inhibitors of LRRK2, a protein kinase mutated in Parkinson's disease. *Biochem. J.* **2009**, *424*, 47−60.

(30) Liu, M.; Kang, S.; Ray, S.; Jackson, J.; Zaitsev, A. D.; Gerber, S. A.; Cuny, G. D.; Glicksman, M. A. Kinetic, mechanistic, and structural modeling studies of truncated wild-type leucine-rich repeat kinase 2 and the G2019S mutant. *Biochemistry* **2011**, *50*, 9399−9408.

(31) Cavasotto, C. N.; Phatak, S. S. Homology modeling in drug discovery: current trends and applications. *Drug Discovery Today* **2009**, *14*, 676−683.

(32) Grant, M. A. Protein structure prediction in structure-based ligand design and virtual screening. *Comb. Chem. High Throughput Screening* **2009**, *12*, 940−960.

(33) Cavasotto, C. N. Homology models in docking and high-throughput docking. *Curr. Top. Med. Chem.* **2011**, *11*, 1528−1534.
(34) Bairoch, A.; Boeckmann, B.; Ferro, S.; Gasteiger, E. Swiss-Prot: juggling between evolution and stability. *Briefings Bioinf.* **2004**, *5*, 39−55.
(35) Altschul, S. F.; Madden, T. L.; Schäffer, A. A.; Zhang, J.; Zhang, Z.; Miller, W.; Lipman, D. J. Gapped BLAST and PSI-BLAST: a new generation of protein database search programs. *Nucleic Acids Res.* **1997**, *25*, 3389−3402.
(36) *MOE*, version 2009.10; Chemical Computing Group Inc.: Montreal, Canada.
(37) Wang, T.; Duffy, J. P.; Wang, J.; Halas, S.; Salituro, F. G.; Pierce, A. C.; Zuccola, H. J.; Black, J. R.; Hogan, J. K.; Jepson, S.; Shlyakter, D.; Mahajan, S.; Gu, Y.; Hoock, T.; Wood, M.; Furey, B. F.; Frantz, J. D.; Dauffenbach, L. M.; Germann, U. A.; Fan, B.; Namchuk, M.; Bennani, Y. L.; Ledeboer, M. W. Janus kinase 2 inhibitors. Synthesis and characterization of a novel polycyclic azaindole. *J. Med. Chem.* **2009**, *52*, 7938−7941.
(38) Covy, J. P.; Giasson, B. I. Identification of compounds that inhibit the kinase activity of leucine-rich repeat kinase 2. *Biochem. Biophys. Res. Commun.* **2009**, *378*, 473−477.
(39) *Maestro*; Schrödinger, Inc.: New York, 2009.
(40) Gould, C.; Wong, C. F. Designing specific protein kinase inhibitors: insights from computer simulations and comparative sequence/structure analysis. *Pharmacol. Ther.* **2002**, *93*, 169−178.
(41) Caffrey, D. R.; Lunney, E. A.; Moshinsky, D. J. Prediction of specificity-determining residues for small-molecule kinase inhibitors. *BMC Bioinf.* **2008**, *9*, 491−505.
(42) Huang, D.; Zhou, T.; Lafleur, K.; Nevado, C.; Caflisch, A. Kinase selectivity potential for inhibitors targeting the ATP binding site: a network analysis. *Bioinformatics* **2010**, *26*, 198−204.
(43) Posy, S. L.; Hermsmeier, M. A.; Vaccaro, W.; Ott, K. H.; Todderud, G.; Lippy, J. S.; Trainor, G. L.; Loughney, D. A.; Johnson, S. R. Trends in kinase selectivity: insights for target class-focused library screening. *J. Med. Chem.* **2011**, *54*, 54−66.
(44) Martin, E.; Mukherjee, P.; Sullivan, D.; Jansen, J. Profile-QSAR: a novel meta-QSAR method that combines activities across the kinase family to accurately predict affinity, selectivity, and cellular activity. *J. Chem. Inf. Model.* **2011**, *51*, 1942−1956.
(45) Anderson, P. C; De Sapio, V.; Turner, K. B.; Elmer, S. P.; Roe, D. C.; Schoeniger, J. S. Identification of binding specificity-determining features in protein families. *J. Med. Chem.* **2012**, *55*, 1926−1939.
(46) Manning, G.; Whyte, D. B.; Martinez, R.; Hunter, T.; Sudarsanam, S. The protein kinase complement of the human genome. *Science* **2002**, *298*, 1912−1934.
(47) Korr, D.; Toschi, L.; Donner, P.; Pohlenz, H. D.; Kreft, B.; Weiss, B. LRRK1 protein kinase activity is stimulated upon binding of GTP to its Roc domain. *Cell. Signalling* **2006**, *18*, 910−920.
(48) Galkin, A. V.; Melnick, J. S.; Kim, S.; Hood, T. L.; Li, N.; Li, L.; Xia, G.; Steensma, R.; Chopiuk, G.; Jiang, J.; Wan, Y.; Ding, P.; Liu, Y.; Sun, F.; Schultz, P. G.; Gray, N. S.; Warmuth, M. Identification of NVP-TAE684, a potent, selective, and efficacious inhibitor of NPM-ALK. *Proc. Natl. Acad. Sci. U.S.A.* **2007**, *104*, 270−275. Erratum in *Proc. Natl. Acad. Sci. U.S.A.* **2007**, *104*, 2025.
(49) Anderson, D. R.; Meyers, M. J.; Vernier, W. F.; Mahoney, M. W.; Kurumbail, R. G.; Caspers, N.; Poda, G. I.; Schindler, J. F.; Reitz, D. B.; Mourey, R. J. Pyrrolopyridine inhibitors of mitogen-activated protein kinase activated protein kinase 2 (MK-2). *J. Med. Chem.* **2007**, *50*, 2647−2654.
(50) Huggins, D. J.; Sherman, W.; Tidor, B. Rational approaches to improving selectivity in drug design. *J. Med. Chem.* **2012**, *55*, 1424−1444.
(51) Leach, A. G.; Jones, H. D.; Cosgrove, D. A.; Kenny, P. W.; Ruston, L.; MacFaul, P.; Wood, J. M.; Colclough, N.; Law, B. Matched molecular pairs as a guide in the optimization of pharmaceutical properties; a study of aqueous solubility, plasma protein binding and oral exposure. *J. Med. Chem.* **2006**, *49*, 6672−6682.
(52) Peltason, L.; Bajorath, J. SAR index: quantifying the nature of structure−activity relationships. *J. Med. Chem.* **2007**, *50*, 5571−5578.
(53) Wassermann, A. M.; Bajorath, J. Chemical substitutions that introduce activity cliffs across different compound classes and biological targets. *J. Chem. Inf. Model.* **2010**, *50*, 1248−1256.
(54) Peltason, L.; Bajorath, J. Computational analysis of activity and selectivity cliffs. *Methods Mol. Biol.* **2011**, *672*, 119−132.
(55) Griffen, E.; Leach, A. G.; Robb, G. R.; Warner, D. J. Matched molecular pairs as a medicinal chemistry tool. *J. Med. Chem.* **2011**, *54*, 7739−7750.
(56) Seebeck, B.; Wagener, M.; Rarey, M. From activity cliffs to target-specific scoring models and pharmacophore hypotheses. *ChemMedChem* **2011**, *6*, 1630−1639.
(57) Scherrmann, J. M. Expression and function of multidrug resistance transporters at the blood−brain barriers. *Expert Opin. Drug Metab. Toxicol.* **2005**, *1*, 233−246.
(58) Schinkel, A. H. P-Glycoprotein, a gatekeeper in the blood−brain barrier. *Adv. Drug Delivery Rev.* **1999**, *36*, 179−194.
(59) Wang, J.; Cieplak, P.; Kollman, P. A. How well does a restrained electrostatic potential (RESP) model perform in calculating conformational energies of organic and biological molecules? *J. Comput. Chem.* **2000**, *21*, 1049−1074.
(60) Thompson, J. D.; Higgins, D. G.; Gibson, T. J. CLUSTAL W: improving the sensitivity of progressive multiple sequence alignment through sequence weighting, position specific gap penalties and weight matrix choice. *Nucleic Acids Res.* **1994**, *22*, 4673−4680.
(61) *Pipeline Pilot*, version 7.5; Accelrys Inc.: San Diego, CA.
(62) Rogers, D.; Hahn, M. Extended-connectivity fingerprints. *J. Chem. Inf. Model.* **2010**, *50*, 742−754.